

A PARAMETRIC WIND-PRESSURE RELATIONSHIP FOR RANKINE VS NON-RANKINE CYCLOSTROPHIC VORTICES

Vincent T. Wood, NOAA/National Severe Storms Laboratory, and Luther W. White, Dept. of Mathematics, University of Oklahoma, Norman, Oklahoma

OBJECTIVES

- To develop a parametric model of tangential wind and pressure profiles by applying the existing parametric Wood-White model to the cyclostrophic wind-pressure relationship of an assumed axisymmetric vortex.
- To compare the non-Rankine* vortex's varying tangential and cyclostrophic pressure profiles to those of the Rankine vortex.

*RANKINE VS. NON-RANKINE VORTICES

- The idealized Rankine-combined vortex is characterized by a core of solid-body rotation [wherein tangential velocity (v) ~ radius (r)], surrounded by an outer region of potential flow (wherein $v \sim r^{-1}$). For convenience, the word "combined" may be dropped.
- The "non-Rankine vortex" may be defined as a viscous vortex which exhibits a smooth transition between solid-body rotation and potential flow that encompasses the annular zone of the velocity maximum, resembling the viscous Burgers-Rott tangential velocity profile.

WOOD-WHITE (V_{WW}) PARAMETRIC WIND PROFILE

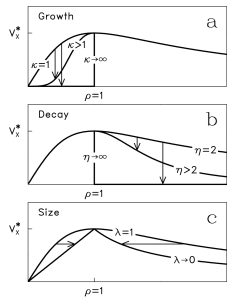
$$V_{WW}^* \equiv \frac{V_{WW}(\rho; \mathbf{m})}{V_X} = \frac{\eta^{\lambda} \rho^{\kappa}}{(\eta - \kappa + \kappa \rho^{\eta/\lambda})^{\lambda}} \quad (1)$$

where V_X is max tangential wind, R_X is radius of V_X , $\rho \equiv r/R_X$, normalized radius from vortex center, κ the *growth* parameter that controls the shape of the inner profile near vortex center (Fig. 1), η the *decay* parameter that controls the shape of the outer profile beyond $\rho=1$, and λ the *size* parameter that controls the radial width of the profile straddling V_X .

Special case: As $\lambda \rightarrow 0$, the WW tangential velocity profile coincides with the Rankine tangential velocity profile (Fig. 1c), given by

$$\lim_{\lambda \rightarrow 0} V_{WW}^* = V_{RV}^* = \begin{cases} \rho^{\kappa}, & \rho \leq 1, \\ \rho^{\kappa-\eta}, & \rho \geq 1. \end{cases} \quad (2)$$

FIG. 1. Radial profiles of V_{WW}^* as a function of (a) κ , (b) η , and (c) λ .



CYCLOSTROPHIC WIND BALANCE

$$\alpha_o \frac{\partial P(r)}{\partial r} = \frac{V_C^2(r)}{r} \quad (3)$$

where $V_C(r)$ is cyclostrophic (tangential) velocity, $P(r)$ radial pressure fluctuation from that of the motionless, equilibrium state multiplied by the constant specific volume of air α_o .

Radial integration of (3) from large radius to $r=0$ yields the pressure deficit for the non-Rankine vortex (WW) in (1):

$$\Delta P_{WW}^*(\rho) \equiv \frac{\Delta P_{WW}(\rho)}{\alpha_o^{-1} V_X^2} = \eta^{-2\lambda} \int_{\infty}^{\rho} \frac{s^{2(\kappa-1)}}{[\eta - \kappa + \kappa s^{(\eta/\lambda)}]^2} ds \quad (4)$$

and for the Rankine vortex (RV):

$$\lim_{\lambda \rightarrow 0} \Delta P_{WW}^*(\rho) = \Delta P_{RV}^*(\rho) \equiv \frac{\Delta P_{RV}(\rho)}{\alpha_o^{-1} V_X^2} = \begin{cases} \int_1^{\rho} s^{2\kappa-1} ds + \int_{\infty}^1 s^{2(\kappa-\eta)-1} ds = \frac{\rho^{2\kappa}-1}{2\kappa} + \frac{1}{2(\kappa-\eta)}, & \rho \leq 1 \\ \int_{\infty}^{\rho} s^{2(\kappa-\eta)-1} ds = \frac{\rho^{2(\kappa-\eta)}}{2(\kappa-\eta)}, & \rho \geq 1 \end{cases} \quad (5)$$

where s is a dummy variable for the integration.

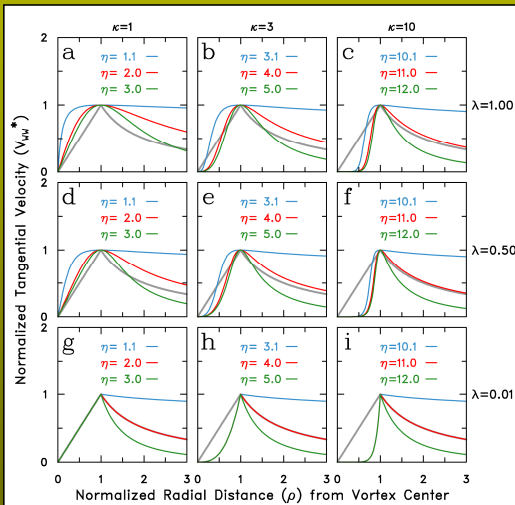


FIG. 2. Radial profile families of V_{WW}^* for selected values of κ, η, λ . Three profile families in each panel are indicated by three different values of η . The gray curve represents the Rankine velocity profile for comparison. Normalized radial distance is represented by $\rho \equiv r/R_X$. [From Wood and White (JAS, 2011).]

Fig. 3a shows radial profiles of the normalized Rankine (gray curve) and non-Rankine (colored curves) tangential velocities for comparison.

Fig. 3b presents the corresponding pressure deficit profiles calculated from (4) and (5).

Different *inner* and *outer* velocity profiles controlled by different λ values have an important influence on the behavior of pressure deficit profiles.

As $\lambda \rightarrow 0$, the non-RV pressure profile coincides with the RV pressure profile.

Vortex A (red curve) has twice the central pressure deficit of the RV, owing to the broadly peaked profile of vortex A.

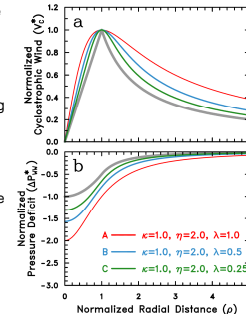


FIG. 3. Radial profiles of non-Rankine vortices A, B and C as a function of λ . Radial profile of Rankine vortex (gray curve) is indicated for comparison.

Fig. 4a shows radial profiles of the normalized Rankine (gray curve) and non-Rankine (colored curves) tangential velocities for comparison.

Fig. 4b presents the corresponding pressure deficit profiles calculated from (4) and (5).

Different *inner* velocity profiles controlled by different κ values have an important influence on the behavior of pressure deficit profiles.

As $\lambda \rightarrow 0$, the non-RV pressure profile coincides with the RV pressure profile.

Vortex D (red curve) has the central pressure deficit about half that of the RV, owing to the drastic reduced tangential velocity profile inside the radius of the maximum.

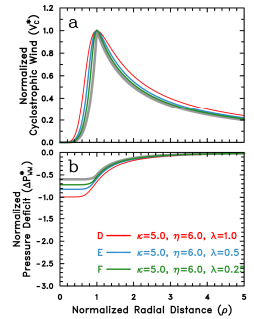


FIG. 4. Radial profiles of non-Rankine vortices D, E and F as a function of κ . Radial profile of Rankine vortex (gray curve) is indicated for comparison.

Fig. 5a shows radial profiles of the normalized Rankine (gray curve) and non-Rankine (colored curves) tangential velocities for comparison.

Fig. 5b presents the corresponding pressure deficit profiles calculated from (4) and (5).

Different *outer* velocity profiles controlled by different η values have an important influence on the behavior of pressure deficit profiles.

As $\lambda \rightarrow 0$, the non-RV pressure profile coincides with the RV pressure profile.

Vortex G (red curve) has twice the central pressure of the RV, owing to the slow decay of the outer profile.

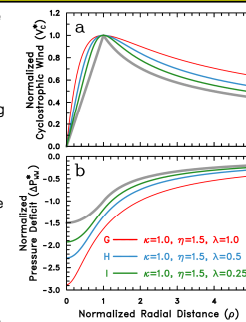


FIG. 5. Radial profiles of non-Rankine vortices G, H and I as a function of η . Radial profile of Rankine vortex (gray curve) is indicated for comparison.

Fig. 6a shows radial profiles of the normalized Rankine (gray curve) and non-Rankine (colored curves) tangential velocities for comparison.

Fig. 6b presents the corresponding pressure deficit profiles calculated from (4) and (5).

Different *outer* velocity profiles controlled by different η values have an important influence on the behavior of pressure deficit profiles.

As $\lambda \rightarrow 0$, the non-RV pressure profile coincides with the RV pressure profile.

Vortex J (red curve) has twice the central pressure of the RV, owing to the quick decay of the outer profile.

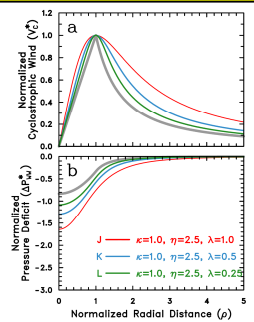


FIG. 6. Radial profiles of non-Rankine vortices J, K and L as a function of η . Radial profile of Rankine vortex (gray curve) is indicated for comparison.

CONCLUSIONS

- Analytical results show that the shape velocity parameters control different shape profiles that in turn have an important modulating influence on the behavior of realistic tangential wind and corresponding pressure deficit profiles.
- When compared to the non-Rankine vortex's pressure deficit profiles for a given tangential velocity maximum, the Rankine's pressure deficit profiles are mismatched because the Rankine's tangential wind profile's unrealistic cusp at the radius of the maximum remains unchanged and is not able to match the wind maximum, as commonly seen in various observations.
- It is suggested that the Rankine vortex model may not provide an analytical model for the observed tangential wind and pressure structures in dust devils, waterspouts, tornadoes, and mesocyclones.



26th Conference on Severe Local Storms
 American Meteorological Society
 5-8 November 2012, Nashville, TN
 Contact: Vincent.Wood@noaa.gov